Impact parameter and energy dependence of observables in intermediate energy heavy-ion reactions

M. Betty Tsang, George F. Bertsch, William G. Lynch, and Mitsuru Tohyama
National Superconducting Cyclotron Laboratory, Michigan State University, East Lansing, Michigan 48824
(Received 24 March 1989)

The dependence of various measurable properties of heavy-ion collisions is calculated with the Boltzmann equation, in an attempt to find the best observables to determine the impact parameter in a collision. The observables considered are nucleon multiplicity, longitudinal momentum transfer, angular momentum transfer, projectile mass loss, and projectile energy loss. Systems studied in detail include the $^{14}N+^{154}Sm$ reaction at $E/A=35$ MeV, the $^{40}Ar+^{197}Au$ reaction at $E/A=60$ MeV, and the $^{16}O+^{197}Au$ reaction at $E/A=90$ MeV where some experiments have been performed with reaction filters. The energy and impact parameter dependence of nucleon multiplicity distributions have also been studied for the mass symmetric $^{40}Ar+^{40}Ar$ and asymmetric $^{16}O+^{197}Au$ systems at energies ranging from $E/A=35$ to 400 MeV. These calculations suggest that the mean multiplicity of fast nucleons and the linear momentum transferred to the target residue are relatively insensitive to the impact parameter at small impact parameters and incident energies below $E/A\leq 60$ MeV. These nucleon multiplicity distributions become more sensitive to impact parameters with increasing incident energy and may provide rather accurate impact parameter information for incident energies as large as $E/A\approx 90$ MeV.

I. INTRODUCTION

To interpret experimental data, it is often important to know the impact parameter of the collision, and the excitation energy and angular momentum transferred to a heavy reaction residue, should one survive the collision. Information about these quantities is obtained most frequently from experimental observables, such as the multiplicities of charged particles,[1,2] γ rays,[3,4] or neutrons,[5,6] or the velocity of heavy reaction residues.[7,8] Total charged particle multiplicities have been used extensively at high energies $E/A\geq 200$ MeV to indicate the centrality of the collision.[1,2] For low incident energies, $E/A\leq 20$ MeV, the multiplicities of neutrons[5,6] and γ rays[3,4] from the reaction residue can supply similar information. The optimum choice of observables for intermediate energy reactions, 20 MeV $\leq E/A\leq 200$ MeV, is not clear. Some guide to the properties of such reaction filters, however, may be obtained from calculations using presently available reaction models.

To explore the properties of reaction filters in this energy domain, we have performed calculations with the Boltzmann equation[9-12] for several systems. We have calculated experimental observables such as the linear and angular momentum transferred to the target residue, the multiplicities and momentum distributions of emitted nucleons, and properties of the projectile-like residues predicted in collisions at large impact parameters. Some numerical details of the calculations are described in Sec. II. The results of calculations for individual systems are described in Sec. III. A summary of the results is provided in Sec. IV.

II. DETAILS OF THE CALCULATIONS

The calculations were performed by numerically solving the Boltzmann equation, given below, which describes the time evolution of the Wigner function $f(\mathbf{r},\mathbf{k},t)$ in phase space:[9-12]

$$\frac{\partial f_1}{\partial t}+\mathbf{v}\cdot\nabla_r f_1-\nabla_r U\cdot\nabla_p f_1=\frac{4}{(2\pi)^3}\int d^3k_2 d^3k_3 d\Omega\,\sigma_{nn}(\Omega)v_{12}$$
$$\times[f_3 f_4(1-f_1)(1-f_2)-f_1 f_2(1-f_3)(1-f_4)]\delta^3(\mathbf{k}_1+\mathbf{k}_2-\mathbf{k}_3-\mathbf{k}_4)\ . \quad (1)$$

Here, $\sigma_{nn}(\Omega)$ and v_{12} are the differential cross section and relative velocity for the colliding nucleons, and U is the mean-field potential approximated by

$$U(\rho)=-356\rho/\rho_0+303(\rho/\rho_0)^{7/6}\ (\text{MeV})\ . \quad (2)$$

The nuclear mean-field defined by Eq. (2) reproduces nuclear matter saturation properties and gives a compressibility coefficient of $K=200$ MeV. For most of the calculations presented here, $4\pi\sigma_{nn}(\Omega)$ is taken to be 41 mb and is isotropic.[13] To explore the influence of the Coulomb repulsion between protons, we also used a modified Boltzmann code which distinguishes protons from neutrons. The mean field in this modified code includes the Coulomb potential and a symmetry potential of the form

$$U_{\text{sym}}=32\frac{\rho_n-\rho_p}{\rho_0}\tau_z\ (\text{MeV}) \quad (3)$$

in addition to the mean field defined by Eq. (2). Here, ρ_n and ρ_p are the neutron and proton densities and τ_z is the isospin operator with eigenvalues $+1$ and -1 for neutrons and protons, respectively. Numerical solutions to Eq. (1) were obtained by propagating test particles according to Newtonian mechanics. The mean-field and the Pauli blocking factors in the collision integral were calculated with distribution functions which were ensemble averaged over 100 parallel simulations.[11]

Calculations were initiated with the surfaces of the projectile and target separated by 2 fm. The test particles are distributed spatially within the projectile and target according to spherical distributions with a radius parameter $r_0 = 1.12$ fm. The momenta are obtained within a local Thomas-Fermi approximation using a mean-field potential defined on a grid with a cell size of 1 fm^3.[11] The density distributions provided by this procedure for a ^{154}Sm nucleus are compared in Fig. 1 to the predictions of a spherical Hartree-Fock calculation.[14] The solid line denotes the density provided by the Hartree-Fock calculation; the dashed line in the figure designates the density provided by the Thomas-Fermi approximation, if one does not distinguish between protons and neutrons and does not include the Coulomb repulsion between protons; the open points are obtained when the Coulomb mean field and the symmetry potential are included in the calculation. The densities predicted by the Thomas-Fermi prescription and the spherical Hartree-Fock calculation are similar at high density $\rho \geq 0.4\rho_0$. In the nuclear surface, however, the local Thomas-Fermi method provides densities which are considerably less than the results of the Hartree-Fock calculation, partly due to the absence of barrier penetration effects in the Thomas-Fermi method. Both the sharp surfaces and the lack of deformation effects cause interactions at large impact parameters, (e.g., $b \geq 9$ fm for ^{14}N + ^{154}Sm at $E/A = 35$ MeV) to be somewhat underestimated by the present calculations. These surface effects should be much less important for small impact-parameter collisions.

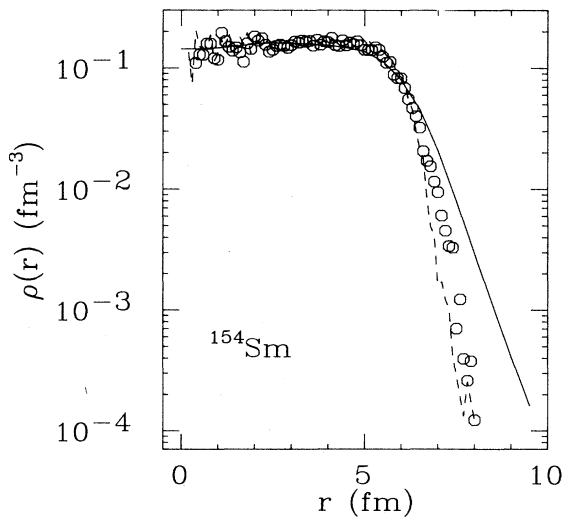

FIG. 1. Density distribution for a ^{154}Sm nucleus. The open points designate the density provided by the Boltzmann calculation, which includes the Coulomb mean-field potential. The dashed line corresponds to the density from the Boltzmann calculation without the Coulomb mean field. The density provided by a spherical Hartree-Fock calculation (Ref. 14) is indicated by the solid line.

For each simulation, we examined the phase-space distribution of nucleons at various time intervals after the start of the collision. In the analysis of the simulations, individual nucleons are assumed to be contained in a fragment if they have a potential energy less than -6 MeV; otherwise they are assumed to propagate freely. (This prescription provides observables which agree, to within a few percent, with those obtained by simpler procedure[15] such as drawing a sphere of radius $R = 1.4A^{1/3}$ about the target residue.) The observables in most calculations were evaluated at a time interval long enough for the fast unbound nucleons and the bound residues to be clearly separated. In collisions where more than two bound fragments were produced, however, the observables were occasionally evaluated before the target-like residue was fully isolated so that all the slow bound fragments would be kept within the grid upon which the mean-field potential was evaluated. In such cases, the velocity, mass, and angular momentum of the target-like residue presented here are less accurate.

In an effort to identify accurate parameter filters, we have calculated the impact-parameter dependence of the multiplicities of nucleons with energies greater than 5 MeV, and the mass, the velocity parallel to the beam axis, and the total angular momentum of heavy target-like residues. In our calculations, such residues survive collisions between asymmetric reaction partners for energies below $E/A = 100$ MeV. We have also calculated the impact-parameter dependence of the mean transverse momentum and the enhancement of nucleon emission patterns in the reaction plane for the ^{14}N + ^{154} Sm system at $E/A = 35$ MeV, the ^{40}Ar + ^{197}Au system at $E/A = 60$ MeV, and the ^{16}O + ^{197}Au system at $E/A = 90$ MeV. While neither of these latter two observables would be suitable for impact-parameter selection, each may provide useful information about the importance of nucleon-nucleon collisions at intermediate energies.

Within the test-particle approach, the observables are evaluated by treating the test particles as classical particles; quantities like the multiplicity, the residue mass, or the angular momentum of the residue, are normalized by dividing by the number of parallel ensembles. Statistical uncertainties for observables associated with unbound test particles are obtained by assuming statistical fluctuations in the Wigner function to be proportional to the square root of the number of test particles. To describe our results, we choose a Cartesian coordinate system in which the total momentum lies along the positive z axis and the initial orbital angular momentum is parallel to the y axis. In this convention, nucleons, which are scattered to forward angles and experience predominantly attractive (repulsive) momentum transfers, emerge with negative (positive) values of the transverse momentum

P_x. To indicate the extent that nucleon emission is enhanced in the reaction plane, we compute the ratio of the yield of nucleons emitted out of the reaction plane to the yield of nucleons emitted in the reaction plane. For this comparison, both in-plane and out-of-plane yields are integrated over polar angles from 40° to 70°; the out-of-plane yield is integrated over azimuthal angles $60° < \Phi < 120°$ and $240° < \Phi < 300°$, and the in-plane yield is integrated over azimuthal angles, $-30° < \Phi < 30°$ and $150° < \Phi < 210°$.

III. RESULTS OF THE SIMULATIONS

We have simulated collisions between the following systems:

$^{14}N+^{154}Sm$ at $E/A=35$ MeV ,

$^{40}Ar+^{197}Au$ at $E/A=60$ MeV ,

$^{16}O+^{197}Au$ at $E/A=60$, 90, 200, and 400 MeV ,

$^{40}Ar+^{40}Ar$ at $E/A=35$, 60, 100, 200, and 400 MeV .

The choice of systems was partly motivated by the availability of experimental data. For example, experiments have been performed for ^{14}N-induced reactions on heavy targets at incident energies near $E/A=35$ MeV, where the velocity of the heavy reaction residue parallel to the beam axis has been used as an impact-parameter filter.[7,16–18] The transverse momentum distributions of unbound nucleons and projectile-like fragments, emitted in $^{14}N+^{154}Sm$ collisions at $E/A=35$ MeV, have been calculated previously with the Boltzmann equation to compare them with measurements of the circular polarization of coincident γ rays from the target residue.[19,20] In this work, we examine the impact-parameter dependence of observables to search for an appropriate impact-parameter filter for this reaction. We also explore in detail the impact-parameter dependence of observables for ^{40}Ar-induced reactions on ^{197}Au at $E/A=60$ MeV (Ref. 21) and ^{16}O induced reactions on ^{197}Au at $E/A=94$ MeV (Ref. 22) because measurements have been performed for these systems in which the multiplicities of coincident light charged particles were used as a reaction filter. To understand how impact parameter filters based on multiplicity measurements evolve with incident energy, we also performed calculations for the mass symmetric $^{40}Ar+^{40}Ar$ system and the mass asymmetric $^{16}O+^{197}Au$ system for a range of bombarding energies.

A. $^{14}N+^{154}Sm$ at $E/A=35$ MeV

We begin our discussions with the $^{14}N+^{154}Sm$ reaction at $E/A=35$ MeV, where our most extensive set of calculations were performed. Observables for this system were calculated at an elapsed time of 200 fm/c. At this point, a well-defined target-like residue with an approximate mass of 150 can be identified at each impact parameter. The velocity in the beam direction V_r, the angular momentum I, and the mass A_r, of the target residue are shown in Fig. 2 as a function of the impact parameter.

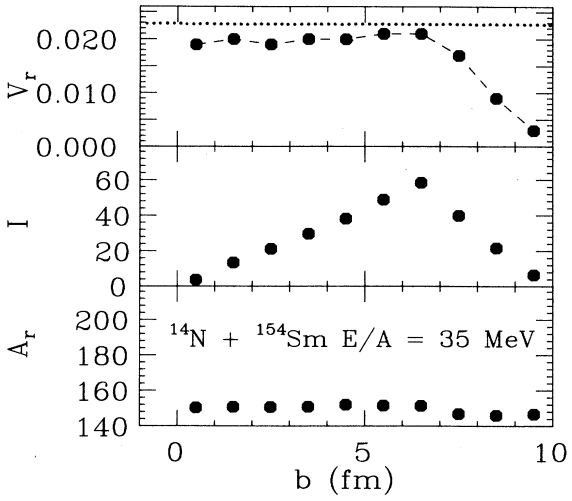

FIG. 2. Predictions for the parallel component of the velocity (upper part), the angular momentum (middle part), and the mass (lower part) of the target-like residue for the $^{14}N+^{154}Sm$ reaction at $E/A=35$ MeV. The dotted line in the upper part of the figure corresponds to the residue velocity consistent with full linear momentum transfer to the target-like residue. The dashed line is drawn to guide the eye.

(Note that the residue mass and angular momentum will continue to decrease with increasing elapsed time of the calculation reflecting the mass and angular momentum loss due to compound evaporation processes.) The dotted line in the uppermost part of the figure denotes the target residue velocity expected for full linear momentum transfer, i.e., complete fusion. The target residue velocity V_r, is surprisingly insensitive to impact parameters for $b \leq 7$ fm. At large impact parameters, $b \geq 7$ fm, where projectile-like residues can be identified in the calculation, V_r drops off sharply with increasing impact parameters. At smaller impact parameters, V_r assumes values that correspond to about 85–90% linear momentum transfer; these values are larger than the most probable linear momentum transfer ($\approx 80\%$) established from systematic measurements on heavy targets,[23] and significantly larger than the values ($\approx 60\%$) reported for this system.[18] Values more comparable to the experimental results are obtained by averaging the target velocity over impact parameter (64%). For $b \leq 7$ fm, the calculations predict that the impact-parameter dependence is reflected most clearly in the angular momentum of the reaction residue; this increases monotonically with b until $b \approx 6.5$ fm then falls off rapidly at larger impact parameters. The maximum transferred angular momentum is about $60\hbar$, much less than the maximum value ($l > 90\hbar$) predicted by the liquid-drop model for nuclei in this mass domain.

Projectile-like fragments are observed at impact parameters larger than 7 fm. In Fig. 3, the mass, deflection angle, energy per nucleon of the projectile-like residue, and the mean transverse momentum P_{xf}/A_f, carried by a nucleon in the projectile-like residue are plotted as solid

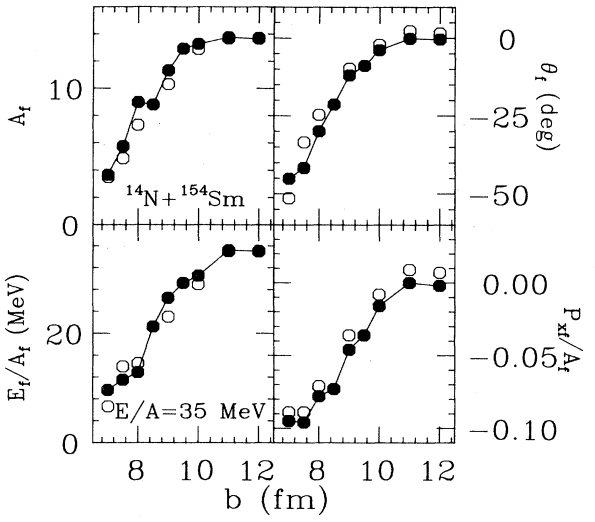

FIG. 3. Predictions for the mass (upper left), angle (upper right), energy per nucleon (lower left), and transverse momentum per nucleon (lower right) of the projectile-like residue for the $^{14}N+^{154}Sm$ reaction at $E/A=35$ MeV. Calculations which include the Coulomb mean field are designated by the open points. Calculations which exclude the Coulomb mean field are designated by the solid points. The solid lines are drawn to guide the eye.

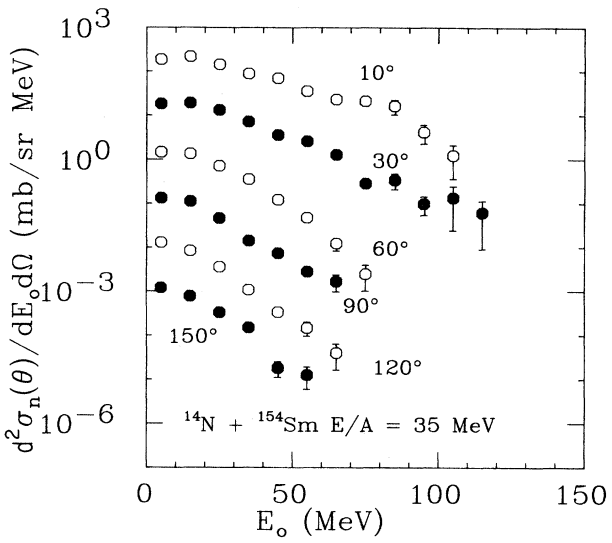

FIG. 4. Nucleon differential cross sections are shown as solid and open points for the $^{14}N+^{154}Sm$ reaction at $E/A=35$ MeV. The normalizations of the cross sections at 10° are correct; the cross sections at successively larger angles are suppressed by successively larger powers of 10.

points for values of the impact parameters greater than 7 fm. The open points are results calculated with the modified Boltzmann code, which includes the Coulomb field for proton test particles. (All the other results in this paper were calculated with the code of Ref. 11, which does not include the Coulomb mean field.) The mass and velocity of the target-like residue parallel to the beam axis (not shown) are only slightly modified by the inclusion of the Coulomb mean field.

For calculations with and without the Coulomb mean field, all four properties of the projectile shown in Fig. 3 increase with impact parameters. Inclusion of the Coulomb mean field leads to a systematic decrease in the projectile-like residue mass, an increase in the deflection angle that is especially pronounced at impact parameters around 8 fm, and positive scattering angles at larger impact parameters, $b \geq 10$ fm. Since fluctuations are important to intermediate mass fragment emission[19,24] but are strongly suppressed by the ensemble averaging used in the computation of the mean field,[24] the connection between the properties of the calculated fragments and the properties of experimentally observed fragments is somewhat tenuous. For this reason, it is questionable whether a comparison of the calculated and measured properties of projectile-like fragments can provide accurate impact-parameter information at any but the most peripheral impact parameters.

Nucleon differential cross sections, shown in Fig. 4, were obtained by summing the nucleon multiplicity distributions over impact parameter. The differential multiplicities for nucleons with laboratory energies greater than 5 MeV were also computed at each impact parameter and then integrated over laboratory angles for three angular ranges 0°–30°, 30°–90°, and 90°–180°. The resulting nucleon multiplicities are shown in Fig. 5. The

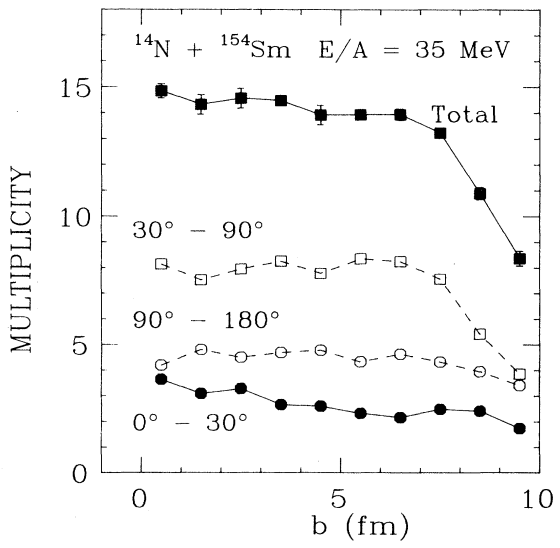

FIG. 5. Nucleon multiplicities for the $^{14}N+^{154}Sm$ reaction at $E/A=35$ MeV are given by the solid and open points in the figure. These multiplicity distributions were integrated over the angular ranges indicated in the figure. Smaller uncertainties occur for points at impact parameters for which more than one calculation was performed. The lines are drawn to guide the eye.

impact-parameter dependence of the total multiplicity is similar to that previously shown for the residue velocity. At large impact parameters, the nucleon multiplicities drop steeply with increasing impact parameter reflecting the decreased overlap of projectile and target. At smaller impact parameter, the nucleon multiplicities are remarkably insensitive to the impact parameter. When one also considers that statistical fluctuations will smear out the correlation between multiplicity and impact parameter, it is clear that the residue velocity provides a better indication of the impact parameter for this reaction. Experimental multiplicity distributions will include particles evaporated from the highly excited target residue. Such evaporation processes are not taken into account by our present calculations. Evaporation calculations are needed to determine whether the inclusion of the yield of such evaporated particles significantly improves the impact-parameter sensitivity of the multiplicity distributions. An even better measure of the impact parameter might be obtained if one should combine multiplicity or residue velocity measurement with a probe, like the γ ray multiplicity, which is sensitive to the angular momentum transfer to the target-like residue.

The shape of the nucleon emission pattern displays some interesting features. In Fig. 6, the ratio of the out-of-plane nucleon cross section to the in-plane nucleon cross section is plotted as a function of the impact parameter. The solid and open points represent nucleon-energy thresholds of $E_0 > 5$ MeV and $E_0 > 20$ MeV, respectively. The calculation indicates that nucleons are emitted preferentially in the reaction plane. Similar results have been reported in Ref. 25. The preference for in-plane emission increases with the energy of the outgoing particle. Such an energy-dependent in-plane enhancement has been observed experimentally for the reaction of $^{14}N+^{197}Au$ at $E/A=30$ MeV.[16] Experimentally, this in-plane enhancement is also observed to increase strongly with the mass of the detected particle.[16] Unfortunately, any mass dependence of the emitted particles cannot be studied in the present model without invoking additional assumptions about the fragment production mechanism. Since these uncertainties in the fragment production mechanism have a significant influence on the in-plane enhancement of particle emission patterns, we have not attempted to determine the sensitivity of the different observables to the azimuthal orientation of the reaction plane.

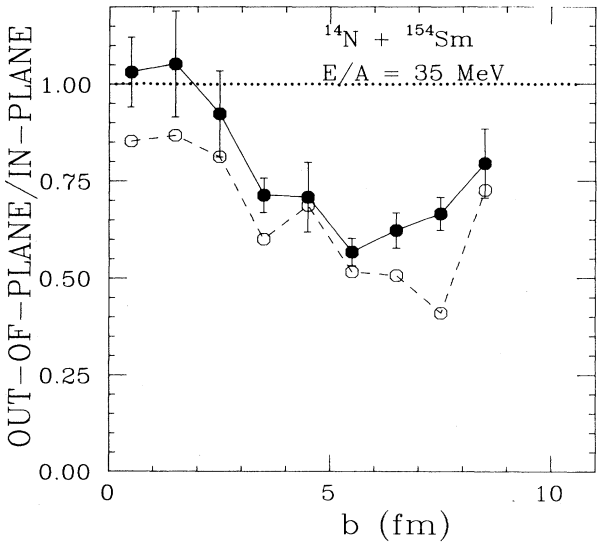

FIG. 6. Ratios of the out-of-plane to in-plane nucleon cross sections are plotted here as functions of the impact parameter for $^{14}N+^{154}Sm$ reactions at $E/A=35$ MeV. These ratios were obtained by integrating the nucleon cross sections over angular ranges specified in Sec. II, and over nucleon energies above energy thresholds of 5 MeV (solid points) and 20 MeV (open points). Smaller uncertainties are assigned to points at impact parameters for which more than one calculation was performed. Statistical uncertainties for the points calculated with the 20 MeV threshold are 30–40% larger than the corresponding uncertainties for the 5-MeV thresholds. The solid and dashed lines are drawn to guide the eye. The dotted line corresponds to the expectation for isotropic emission.

Information about the reaction dynamics is also contained in the mean transverse momentum $\langle P_x \rangle$ of unbound nucleons.[15,26] Solutions of the Boltzmann equation indicate that the mean transverse momentum in intermediate energy heavy-ion collisions is very sensitive to the interplay between the attractive nuclear mean-field and nucleon-nucleon collisions.[15,20] The mean transverse momentum of unbound nucleons, shown in Fig. 7, is negative at all impact parameters for this reaction. The negative values for $\langle P_x \rangle$ are consistent with experimental measurements of the circular polarization of γ rays emitted by the target residue;[20] they suggest the dominance of the attractive nuclear mean field. The mean transverse momentum decreases with increasing impact parameters until a minimum is reached at about 6 fm, then it increases and vanishes at much larger impact parameters. Such a strong impact-parameter dependence clearly illustrates the need to develop a good experimental measure of the impact parameters. At large impact parameters,

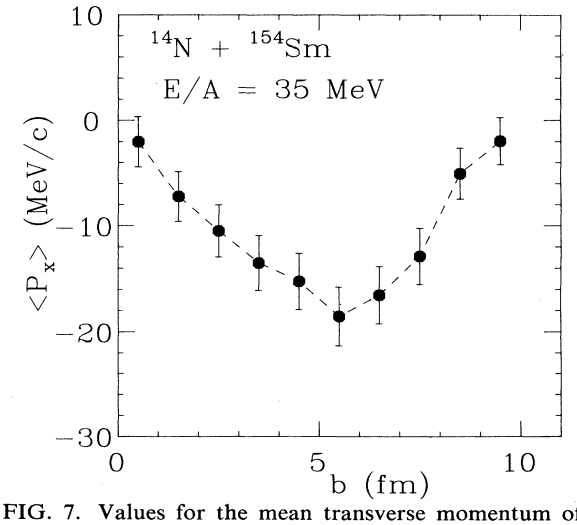

FIG. 7. Values for the mean transverse momentum of unbound nucleons calculated with the Boltzmann equation for $^{14}N+^{154}Sm$ reactions at $E/A=35$ MeV. The line is drawn to guide the eye.

the calculations predict that negative transverse momenta are carried by the projectile-like residues. Due to the subsequent evaporation by projectile-like residues, there is an ambiguity in the magnitude of $\langle P_x \rangle$ one should assign to nucleons or light particles at large impact parameters. To avoid this ambiguity, the mean transverse momenta of Ref. 15 include both the momenta of unbound nucleons and the momenta of nucleons contained in fast bound residues.

While the predictions of the Boltzmann equation are sensitive to the nucleon-nucleon cross section contained in the collision integral, there is presently little experimental information to constrain this nucleon-nucleon cross section. To explore the sensitivity of these predictions to the nucleon-nucleon cross section, additional calculations were performed with a reduced nucleon-nucleon cross section of $4\pi\sigma_{nn}=20$ mb. Comparisons of the nucleon-energy spectra, the nucleon multiplicities, the ratios of out-of-plane to in-plane nucleon cross sections, and the mean transverse momenta are shown in Figs. 8–11 for $4\pi\sigma_{nn}=20$ mb and $4\pi\sigma_{nn}=41$ mb. Nucleon distributions are slightly more forward peaked, and more enhanced in the reaction plane in calculations where the nucleon-nucleon cross section is reduced. The mean transverse momenta are significantly more negative.[15,20] These differences are not unexpected since nucleon-nucleon collisions make the nucleon velocity distributions for this bombarding energy domain more random and isotropic. The overall nucleon multiplicity is also somewhat lower with the reduced nucleon-nucleon cross section, and is more sensitive to impact parameters. The velocity of the heavy residue (not shown) is also somewhat less. In principle, these differences may enable

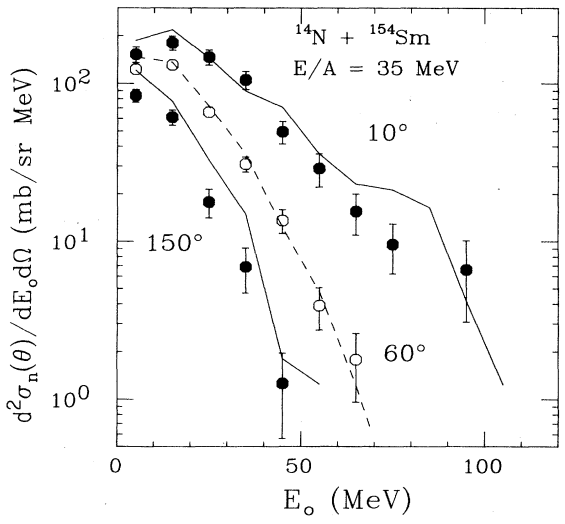

FIG. 8. Nucleon-energy spectra calculated with the Boltzmann equation and a reduced nucleon-nucleon cross section of 20 mb are shown as solid and open points for the ^{14}N+^{154}Sm reaction at $E/A=35$ MeV. The corresponding energy spectra calculated with a nucleon-nucleon cross section of 41 mb are depicted by the solid and dashed lines. The statistical uncertainties for the calculations with the 41-mb nucleon-nucleon cross section are shown in Fig. 4.

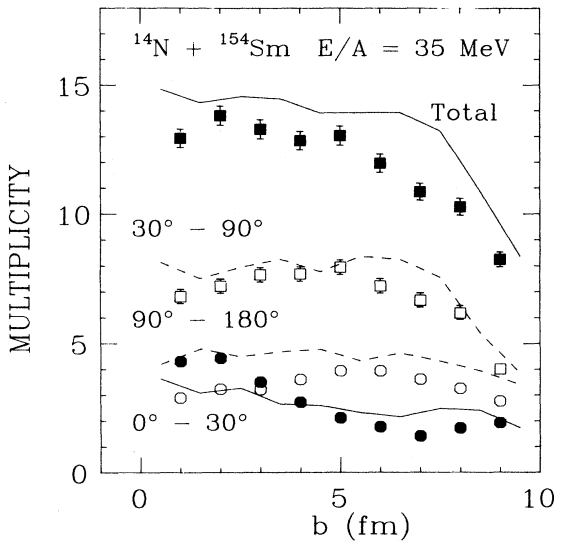

FIG. 9. Nucleon multiplicities for the ^{14}N+^{154}Sm reaction at $E/A=35$ MeV calculated with the Boltzmann equation and a reduced nucleon-nucleon cross section of 20 mb are given by the solid and open points in the figure. The corresponding calculations with a nucleon-nucleon cross section of 41 mb are depicted by the solid and dashed lines. These multiplicity distributions were integrated over the angular ranges indicated in the figure. The statistical uncertainties for the calculations with the 41-mb nucleon-nucleon cross section are shown in Fig. 5.

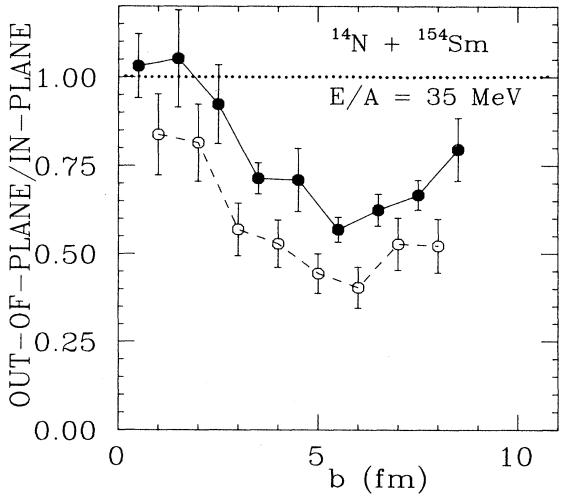

FIG. 10. Ratios of the out-of-plane to in-plane nucleon cross sections calculated with the Boltzmann equation and a nucleon-nucleon cross section of 41 mb are plotted as the solid points for ^{14}N+^{154}Sm reactions at $E/A=35$ MeV. Ratios calculated with a reduced nucleon-nucleon cross section of 20 mb are depicted by the open points. These ratios were obtained by integrating the nucleon cross sections over angles indicated in Sec. II and over nucleon energies above an energy threshold of 5 MeV. The solid and dashed lines are drawn to guide the eye. The dotted line corresponds to the expectation for isotropic emission.

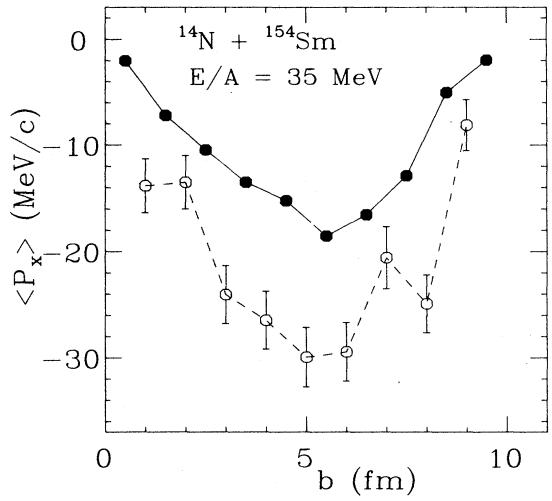

FIG. 11. Values for the mean transverse momentum of unbound nucleons calculated with the Boltzmann equation and a nucleon-nucleon cross section of 41 mb are plotted here as solid points for $^{14}N+^{154}Sm$ reactions at $E/A=35$ MeV. The corresponding calculations with a reduced nucleon-nucleon cross section of 20 mb are given by the open points. Statistical uncertainties for both calculations are about the same. The lines are drawn to guide the eye.

one to determine empirically the most appropriate nucleon-nucleon cross section for these simulations. The strongest sensitivities to the nucleon-nucleon cross section are displayed by the mean transverse momenta and the in-plane enhancement of the nucleon emission patterns. These two observables, however, are strongly impact-parameter dependent, illustrating the importance of establishing reliable measures of the impact parameters.

B. ^{40}Ar+^{197}Au at $E/A=60$ MeV

Calculations were performed for this system for an elapsed time of 150 fm/c for all impact parameters smaller than 10 fm. At 10 fm, the calculation was stopped at 90 fm/c. As shown in the upper half of Fig. 12, well-defined projectile- and target-like residues could be clearly identified in collisions at large impact parameters. At impact parameters $4 \leq b \leq 6$ fm, as shown in the lower half of the figure, more than two bound fragments were frequently observed at the end of the calculation. For these cases, the fragments in the multifragment final state were sometimes not completely separated at an elapsed time of 150 fm/c.

The velocity, angular momentum, and mass of the largest (target-like) residue are shown in Fig. 13 as a function of the impact parameters. The residue velocity V_r decreases smoothly with the impact parameters. At small impact parameters, $b<3$ fm, the residue velocity is at least 80% of the velocity of a residue from a complete fusion reaction. Determinations of the residue velocity from fission folding angle distributions, however, are inconsistent with the existence of such high-velocity residues.[27,28] These calculations could still be reconciled to the experimental data if these highly excited residues do not decay by fission and either decay to heavy residues or decay by unconventional, perhaps multifragment decay modes. The angular momentum of the residue, shown in Fig. 13, has a maximum value of $100\hbar$ at about $b=4$ fm. This value is larger than the maximum value ($l>85\hbar$) predicted by the liquid-drop model. As mentioned previously, between $b=4$ and 6 fm more than two fragments are found in the final state and are not separated in these calculations by an elapsed time of 150 fm/c. The properties of the heavy residue between 4 and 6 fm are therefore somewhat inaccurate.

Excluding the target residue, we have calculated the properties of other bound fragments produced in the simulations. The total mass, average deflection angle, energy per nucleon, and mean transverse momentum per nucleon of these fast bound fragments is shown in Fig. 14. The solid points for $b \geq 7$ fm indicate the values at impact parameters where a single fast fragment is pre-

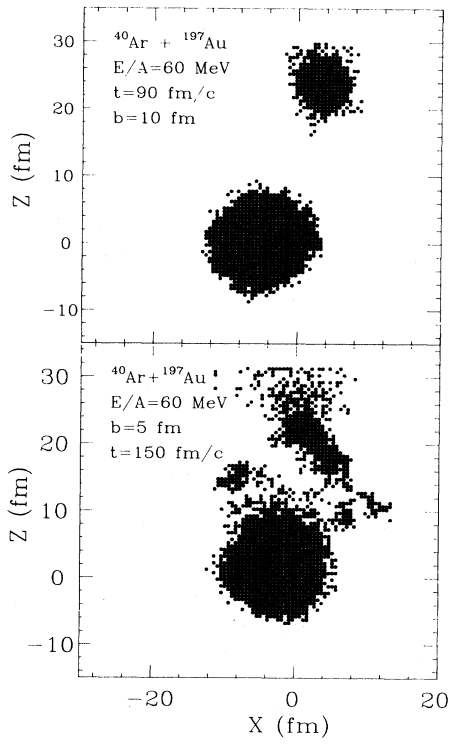

FIG. 12. The locations of bound test particles calculated with the Boltzmann equation Upper half: projectile- and target-like residues can be clearly identified for collisions at an impact parameter of 10 fm and an elapsed time of 90 fm/c. Lower half: more than two bound residues are observed for this collision at an impact parameter of 5 fm and an elapsed time of 150 fm/c. The location of unbound test particles are not plotted in these figures.

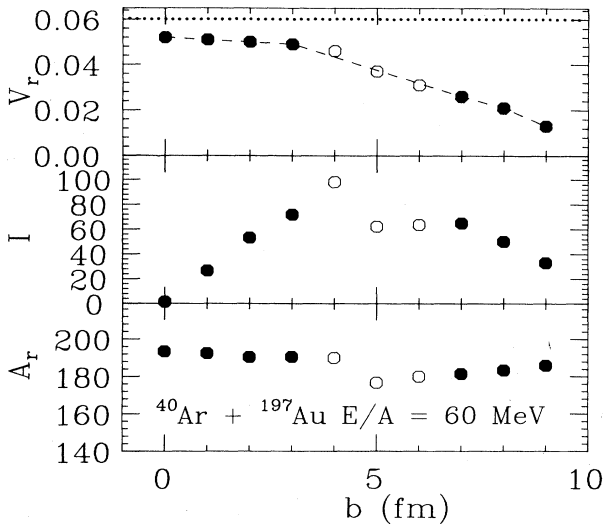

FIG. 13. Predictions for the parallel component of the velocity (upper part), the angular momentum (middle part), and the mass (lower part) of the target-like residue for the $^{40}Ar+^{197}Au$ reaction at $E/A=60$ MeV. The open points correspond to impact parameters where more than one fast bound fragment was produced in the calculations. The solid points denote calculations for which no more than one fast fragment was produced. The dotted line in the upper part of the figure corresponds to the residue velocity which is consistent with the full linear momentum transfer to the target-like residue.

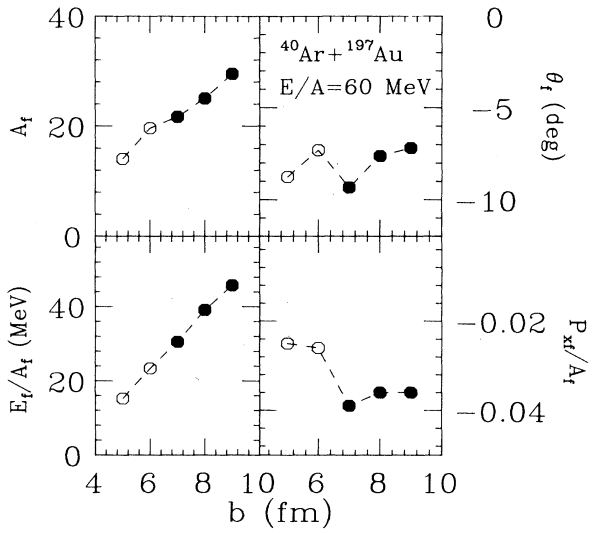

FIG. 14. Predictions for the mass (upper left), angle (upper right), energy per nucleon (lower left), and transverse momentum per nucleon (lower right) of the projectile-like residue for the $^{40}Ar+^{197}Au$ reaction at $E/A=60$ MeV. The open points correspond to impact parameters where more than one fast bound fragment was produced in the calculations. The solid points denote calculations for which no more than one fast fragment was produced.

dicted. The open points for $b \leq 6$ fm indicate the values obtained when more than one fast fragment is predicted; these points were calculated by treating all the nucleons in fast fragments as if they were contained in a single fragment. As shown by the figure, the mean scattering angle of fast bound fragments, $-10°$, is nearly independent of impact parameter. The projectile-like fragment produced at $b \geq 7$ fm is relatively energetic, $E_f/A_f > 20$ MeV. Slower fragments are produced at smaller impact parameters, where the calculation produces multifragment final states.

The calculated nucleon differential cross sections are shown as the open and solid points in Fig. 15. To compare these calculations to experimental data, we have assumed for simplicity that light particle production can be treated by the coalescence approximation[29] and have combined the measured light particle spectra[30] using the relationship

$$\left|\frac{d^2\sigma_n}{dE_0 d\Omega}\right|_{\text{exp}} = 2\frac{d^2\sigma_p}{dE\,d\Omega}\bigg|_{E=E_0+V_{\text{Coul}}} + 4\frac{d^2\sigma_d}{dE\,d\Omega}\bigg|_{E=2E_0+V_{\text{Coul}}} + 9\frac{d^2\sigma_t}{dE\,d\Omega}\bigg|_{E=3E_0+V_{\text{Coul}}} + 9\frac{d^2\sigma_{^3\text{He}}}{dE\,d\Omega}\bigg|_{E=3E_0+2V_{\text{Coul}}} + 16\frac{d^2\sigma_\alpha}{dE\,d\Omega}\bigg|_{E=4E_0+2V_{\text{Coul}}} . \quad (4)$$

This relationship assumes the equality of the neutron and proton production cross sections. The acceleration of protons and light composite nuclei in the Coulomb field of the target residue was approximated by a Coulomb shift $\Delta E = ZV_{\text{Coul}}$ with $V_{\text{Coul}} = 10$ MeV. The factor A^2 that precedes each term (except the first term) in Eq. (4) reflects both the number of primary nucleons in each fragment and the conversion from the fragment energy to the energy of the constituent nucleons. The resulting effective nucleon cross sections are indicated by the solid and dashed lines in Fig. 15. The shape of the energy spectra are well reproduced at all angles. The magnitude of the calculations reproduce well the experimental data at forward angles. At backward angles greater than 70°, however, the calculated spectra exceed the experimental results, with the discrepancy increasing with scattering angle. It is not clear at present whether this indicates a deficiency in the coalescence prescription, a need for a smaller nucleon-nucleon cross section, or a shortcoming in the Boltzmann approach.

The nucleon multiplicity distributions are shown in Fig. 16 as a function of impact parameters. These calcu-

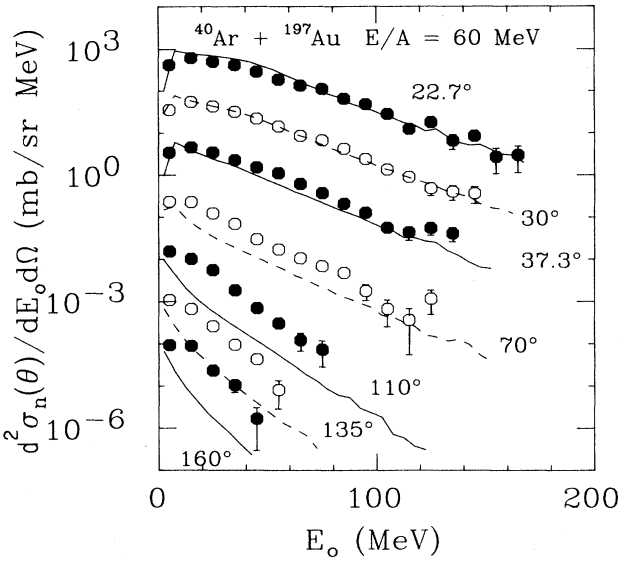

FIG. 15. Nucleon differential cross sections calculated with the Boltzmann equation are shown as solid and open points for the ^{40}Ar+^{197}Au reaction at $E/A=60$ MeV. The normalizations of the cross sections at 22.7° are correct; the cross sections at successively larger angles are suppressed by successively larger powers of 10. The solid and dashed lines correspond to effective nucleon cross sections derived from the experimental data of Ref. 30 according to Eq. (4).

lations suggest that misleading conclusions may be reached if one uses devices which measure the multiplicity exclusively in the forward direction.[21,31] Similar conclusions have been reached from measurements at lower incident energies.[32] Indeed, for this reaction the maximum multiplicities for nucleons emitted to 0°–30°, are

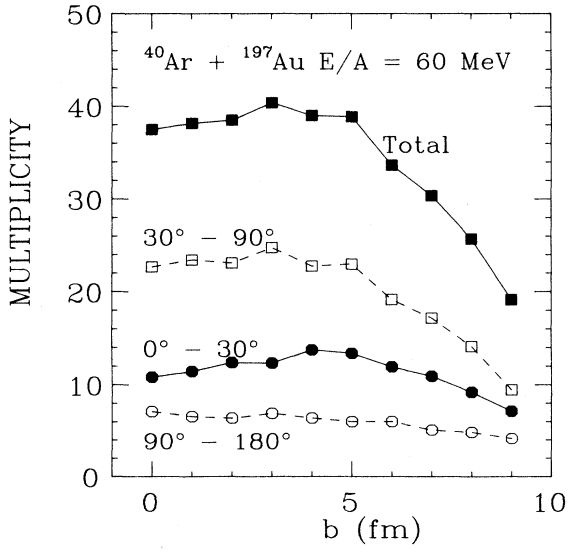

FIG. 16. Nucleon multiplicities for the ^{40}Ar+^{197}Au reaction at $E/A=60$ MeV are given by the solid and open points in the figure. These multiplicity distributions were integrated over the angular ranges indicated in the figure. The lines are drawn to guide the eye.

obtained for intermediate impact parameters $b\approx 4$–5 fm. The calculated multiplicities are remarkably independent of impact parameters at $b<5$ fm. Thus, while more accurate information may be obtained with experimental devices which have a more complete angular coverage, the present calculations suggest that it may not be possible to differentiate between impact parameters less than $b\approx 5$ fm using the multiplicity. Even at larger impact parameters, the relationship between multiplicity and impact parameters can become indefinite due to fluctuations in the multiplicity. The effect of these fluctuations will be reduced, however, if one includes the yields of particles evaporated from the target residue.

We have also computed the ratio of out-of-plane to in-plane differential multiplicities, shown in Fig. 17. The calculations also predict that a larger fraction of the nucleons are emitted in the reaction plane at larger impact parameters. The mean transverse momentum, shown in Fig. 18, is similar in magnitude to that calculated for the ^{14}N+^{154}Sm system. The minimum occurs at an impact parameter of about 5 fm. The emission patterns for the most energetic nucleons are slightly more isotropic for this reaction than for the ^{14}N+^{154}Sm reaction at $E/A=35$ MeV. Two particle correlation measurements for this reaction suggest a much greater isotropy in the nucleon emission patterns.[33,34] This apparent isotropy has been partly attributed to the effects of averaging over the azimuthal angle of the reaction plane, since the azimuthal orientation of the reaction plane is not well defined by such measurements.

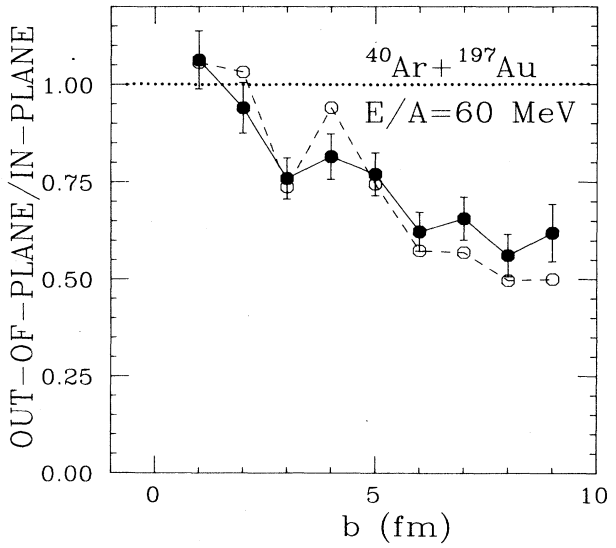

FIG. 17. Ratios of the out-of-plane to in-plane nucleon cross sections are plotted here as functions of the impact parameter for ^{40}Ar+^{197}Au reactions at $E/A=60$ MeV. These ratios were obtained by integrating the nucleon cross sections over angles as discussed in Sec. II, and over nucleon energy subject to energy thresholds of 5 MeV (solid points) and 20 MeV (open points). Statistical uncertainties for the points calculated with the 20-MeV threshold are 30–40% larger than the corresponding uncertainties for the 5-MeV thresholds. The solid and dashed lines are drawn to guide the eye. The dotted line corresponds to the expectation for isotropic emission.

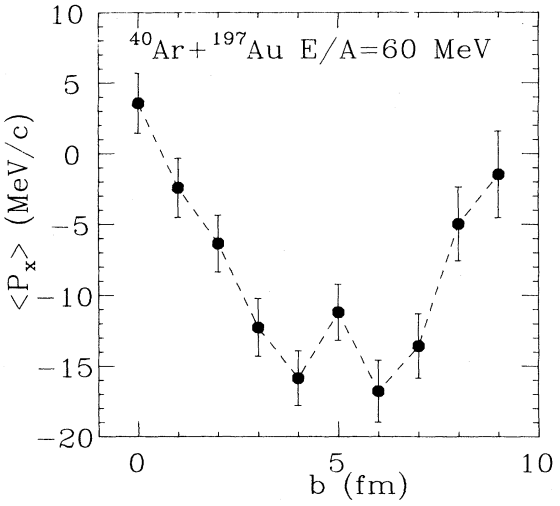

FIG. 18. Values for the mean transverse momentum of unbound nucleons calculated with the Boltzmann equation for ^{40}Ar+^{197}Au reactions at $E/A=60$ MeV. The line is drawn to guide the eye.

C. ^{16}O+^{197}Au at $E/A=60$ and 90 MeV

We first consider the reaction at $E/A=60$ MeV. The observables were calculated for this reaction at an elapsed time of 150 fm/c, by which time a well-defined target residue can be identified at each impact parameter. We confine our discussion of this reaction to the properties of the target residue and the nucleon multiplicities. The properties of the target residue are shown in Fig. 19.

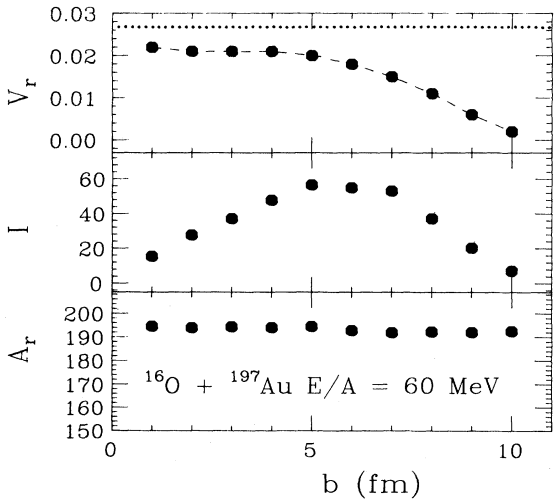

FIG. 19. Predictions for the parallel component of the velocity (upper part), the angular momentum (middle part), and the mass (lower part) of the target-like residue for the ^{16}O+^{197}Au reaction at $E/A=60$ MeV. The dotted line in the upper part of the figure corresponds to the residue velocity consistent with full linear momentum transfer to the target-like residue. The dashed line is drawn to guide the eye.

Qualitatively, the trends are similar to those calculated for the other systems. The residue velocity begins to decrease smoothly at about 5 fm, slightly smaller than for the ^{14}N+^{154}Sm system at $E/A=35$ MeV, and displays a trend that is also similar to that observed for the ^{40}Ar+^{197}Au reaction at $E/A=60$ MeV. The most significant differences with the ^{40}Ar+^{197}Au calculation occur principally at impact parameters near 5 fm, where more than two bound fragments are found in the simulations of the ^{40}Ar+^{197}Au system. The maximum transferred angular momentum is about $60\hbar$ for the ^{16}O+^{197}Au system at $E/A=60$ MeV, much less than the maximum values ($l>80\hbar$) predicted by the liquid-drop model for nuclei in this mass domain. For $b<5$ fm, the residue velocity is insensitive to the impact parameter; only the angular momentum transfer is sensitive to the impact parameter for such small impact parameters.

The impact-parameter dependence of the nucleon multiplicity is shown in Fig. 20. Like the other low-energy systems, the total multiplicity is rather insensitive to impact parameters for impact parameters less than 5 fm, where it saturates at values comparable to the mass number of the projectile. The multiplicity at forward angles ($\theta_{lab}\leq 30°$) is essentially flat for impact parameters less than about 8 or 9 fm.

We turn now to the reaction at $E/A=90$ MeV. The observables for this system were evaluated at an elapsed time of 100 fm/c. A well-defined target-like residue can be identified at each impact parameter. Properties of the target-like residue are shown in Fig. 21. These results are qualitatively similar to those obtained for the ^{14}N+^{154}Sm reaction at $E/A=35$ MeV and the ^{16}O+^{197}Au reaction at $E/A=60$ MeV. Both the linear and angular momentum transfer begin to decrease at smaller values ($b\approx 5$ fm) of the impact parameters than that observed at

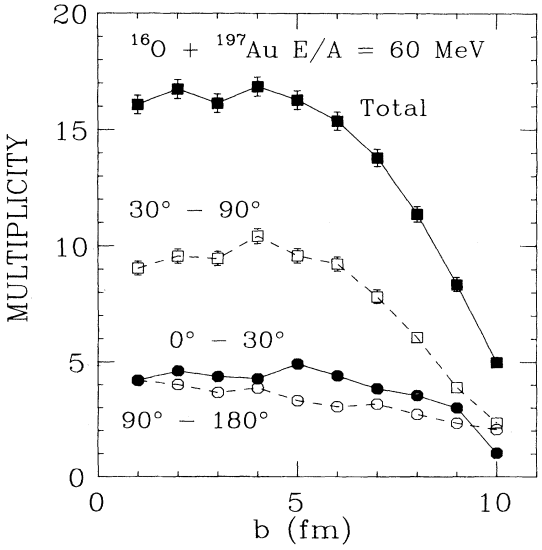

FIG. 20. Nucleon multiplicities for the ^{16}O+^{197}Au reaction at $E/A=60$ MeV are given by the solid and open points in the figure. These multiplicity distributions were integrated over the angular ranges indicated in the figure. The lines are drawn to guide the eye.

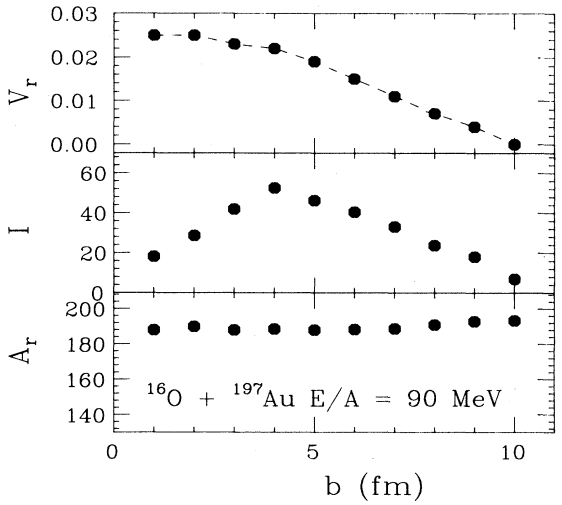

FIG. 21. Predictions for the parallel component of the velocity (upper part), the angular momentum (middle part), and the mass (lower part) of the target-like residue for the $^{16}O+^{197}Au$ reaction at $E/A=90$ MeV. The residue velocity consistent with full linear momentum transfer to the target-like residue lies outside the range of the figure and therefore is not shown.

$E/A=60$ MeV. Of the properties of the target-like residue, only the angular momentum transfer is impact-parameter dependent for impact parameters less than 4 fm. The maximum transferred angular momentum is about $57\hbar$, much less than the maximum values ($l>80\hbar$) predicted by the liquid-drop model. Projectile-like fragments are observed for this reaction at $b\geq 6$ fm. The properties of the projectile-like residual are shown in Fig. 22. Both the energy per nucleon and the mass of the projectile-like fragment increase with increasing impact parameters. Interestingly, the absolute value of the calculated deflection angle does not decrease beyond $-10°$ nor does the energy per nucleon decrease below about 50 MeV, regardless of the impact parameter.

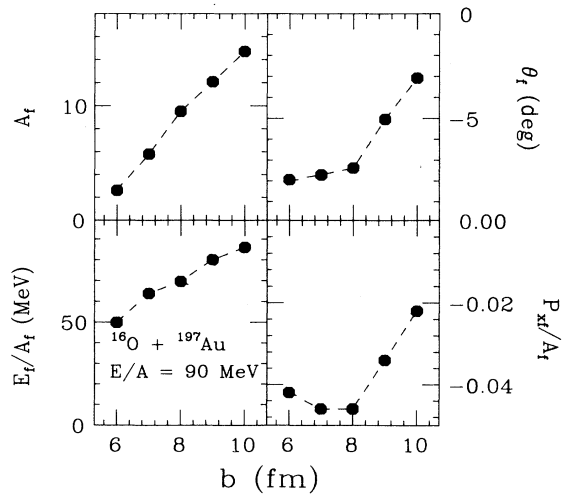

FIG. 22. Predictions for the mass (upper left), angle (upper right), energy per nucleon (lower left), and transverse momentum per nucleon (lower right) of the projectile-like residue for the $^{16}O+^{197}Au$ reaction at $E/A=90$ MeV.

Nucleon-energy spectra predicted by the Boltzmann equation are shown as the solid and open points in Fig. 23. The solid and dashed lines correspond to effective nucleon cross sections obtained by combining data for the $^{16}O+^{197}Au$ system at $E/A=94$ MeV (Ref. 22) according to Eq. (4). The agreement between the calculated and measured spectra is very good. Unfortunately, measurements of the energy spectra are not available at larger scattering angles where the discrepancies between the effective nucleon cross sections and the calculated nucleon spectra could be larger.

The dependence of nucleon multiplicities on impact parameters, is shown in Fig. 24 for different angular ranges. It is noteworthy that the multiplicity at forward (0°–30°) and backward (30°–180°) angular ranges depend differently upon impact parameters. In particular, multiplicities greater than 6 in the forward angular range (0°–30°) occur preferentially at intermediate impact parameters $3<b<8$ fm. On the other hand, a multiplicity greater than 10 in the backward angular range (30°–180°) occurs primarily for more central collisions, $b<6$ fm. The calculations suggest that suitable combinations of forward, backward, and total multiplicities could permit one to bias experimental data alternatively towards small, intermediate, or large impact parameters.

The ratio of the out-of-plane to the in-plane nucleon

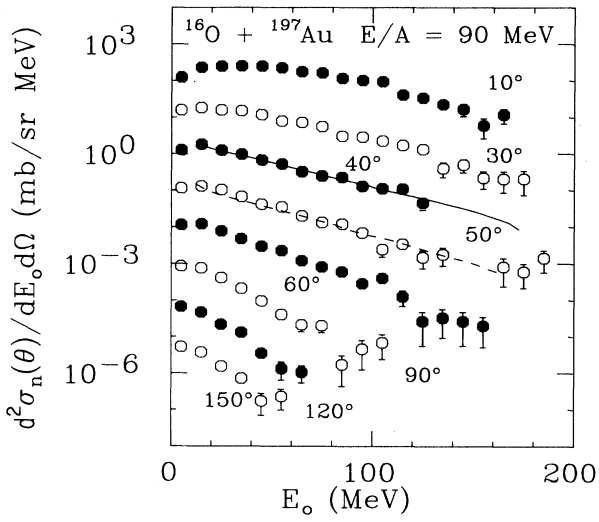

FIG. 23. Nucleon differential cross sections calculated with the Boltzmann equation are shown as solid and open points for the $^{16}O+^{197}Au$ reaction at $E/A=90$ MeV. The normalizations of the cross sections at 10° are correct; the cross sections at successively larger angles are suppressed by successively larger powers of 10. The solid and dashed lines correspond to effective nucleon cross sections at $\theta=40°$ and 50°, respectively, derived from the experimental data of Ref. 22, according to Eq. (4).

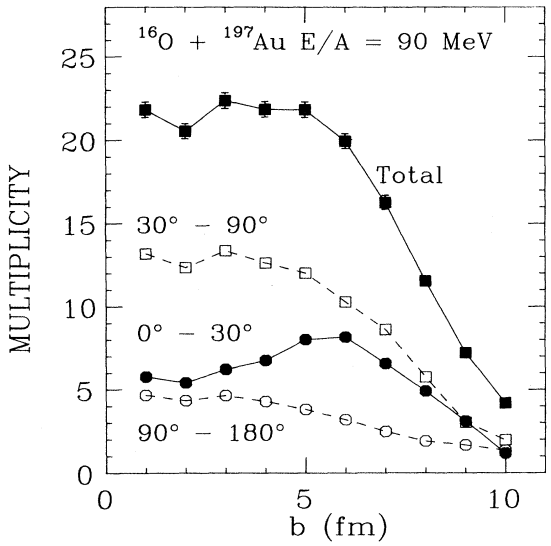

FIG. 24. Nucleon multiplicities for the $^{16}O+^{197}Au$ reaction at $E/A=90$ MeV are given by the solid and open points in the figure. These multiplicity distributions were integrated over the angular ranges indicated in the figure. The lines are drawn to guide the eye.

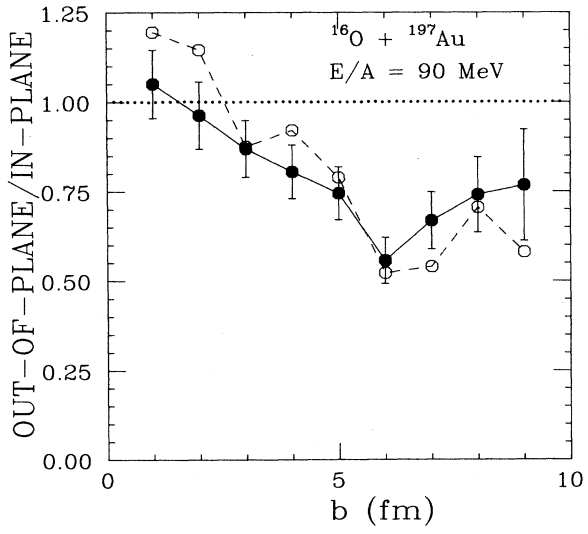

FIG. 25. Ratios of the out-of-plane to in-plane nucleon cross sections are plotted here as functions of the impact parameter for $^{16}O+^{197}Au$ reactions at $E/A=90$ MeV. These ratios were obtained by integrating the nucleon cross sections over the angles as specified in Sec. II and over the nucleon energy subject to energy thresholds of 5 MeV (solid points) and 20 MeV (open points). Statistical uncertainties for the points calculated with the 20-MeV threshold are 30–40% larger than the corresponding uncertainties for the 5-MeV thresholds. The solid and dashed lines are drawn to guide the eye. The dotted line corresponds to the expectation for isotropic emission.

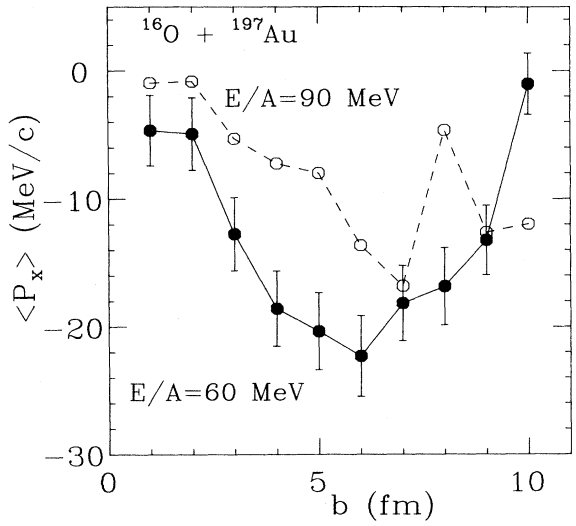

FIG. 26. Values for the mean transverse momentum of unbound nucleons calculated with the Boltzmann equation for $^{16}O+^{197}Au$ reactions at $E/A=60$ and 90 MeV. The lines are drawn to guide the eye. The statistical uncertainties for the latter points are about 15% smaller than the uncertainties at $E/A=60$ MeV.

cross sections is shown in Fig. 25. Particularly for the most energetic nucleons, the out-of-plane nucleon cross sections are slightly enhanced with respect to those in plane at small impact parameters, $b \leq 2$. The ratio of out-of-plane to in-plane nucleon yields decreases with the impact parameter. The mean transverse momenta obtained for collisions at $E/A=90$ MeV, shown in Fig. 26, are significantly less negative at $b \leq 5$ fm than the transverse momenta obtained for the same system at $E/A=60$ MeV; they are also less negative than for the $^{14}N+^{154}Sm$ system at $E/A=35$ MeV. This increase of $\langle P_x \rangle$ with incident energy is a consequence of the increased importance of nucleon-nucleon collisions at higher energies where Pauli blocking effects are less important.

D. The bombarding energy dependence of the nucleon multiplicities

As the bombarding energy is increased, it becomes increasingly advantageous to be able to select the impact parameter using the properties of the unbound nucleons or light particles. To illustrate the evolution of the nucleon multiplicity distributions with the impact parameters, we have calculated the nucleon multiplicity distributions for the symmetric $^{40}Ar+^{40}Ar$ system and the asymmetric $^{16}O+^{197}Au$ system for E/A ranging between 35 and 400 MeV.

We consider first calculations for the $^{40}Ar+^{40}Ar$ system. In these calculations, nucleon multiplicities were evaluated after an elapsed time of 200, 150, 100, 75, and 50 fm/c for calculations performed at the incident energies $E/A=35$, 60, 100, 200, and 400 MeV, respectively. Fusion is predicted to occur only at $b=1$ fm for col-

lisions at $E/A=35$ MeV. At this energy and larger impact parameters, well-formed projectile- and target-like residues can be identified at the end of each calculation. At higher energies, two bound residues occur mainly at large impact parameters; at small impact parameters, many fragments are frequently produced. As an example, Fig. 27 shows a calculation for the $^{40}Ar+^{40}Ar$ system at $E/A=60$ MeV and $b=0$ fm after an elapsed time of 250 fm/c. In this calculation, six separate fragments can clearly be seen. About 30% of the calculations at this impact parameter result in more than two bound fragments.

The total multiplicity and the multiplicity of nucleons emitted at $\theta_{lab} \leq 30°$ are shown in Fig. 28 for the $^{40}Ar+^{40}Ar$ system at four bombarding energies. Like the $^{14}N+^{154}Sm$ system at $E/A=35$ MeV, the total multiplicity for the $^{40}Ar+^{40}Ar$ system at $E/A=35$ MeV is insensitive to impact parameters for small impact parameters. At higher energies, however, the total multiplicity displays a monotonic, almost linear, dependence on impact parameters. The multiplicity at any given parameter grows with incident energy and reaches limiting values consistent with the participant spectator model by $E/A=200$ MeV. Multiplicities calculated at $E/A=400$ MeV (not shown) are about 10% larger and have essentially the same dependence on impact parameters as those calculated at $E/A=200$ MeV.

The multiplicity also shows energy-dependent trends for the $^{16}O+^{197}Au$ reaction. In addition to the calculations at $E/A=60$ and 90 MeV presented previously, calculations were performed at incident energies of $E/A=200$ and 400 MeV. For these reactions, nucleon multiplicity distributions were evaluated after elapsed times of 75 and 50 fm/c, respectively. After this time interval, well-formed projectile- and target-like residues were observed mainly in collisions at large impact parameters. At small impact parameters, multifragment final states were occasionally observed.

The energy dependence of the multiplicity distributions for $^{16}O+^{197}Au$ reactions is shown in Fig. 29. It is in-

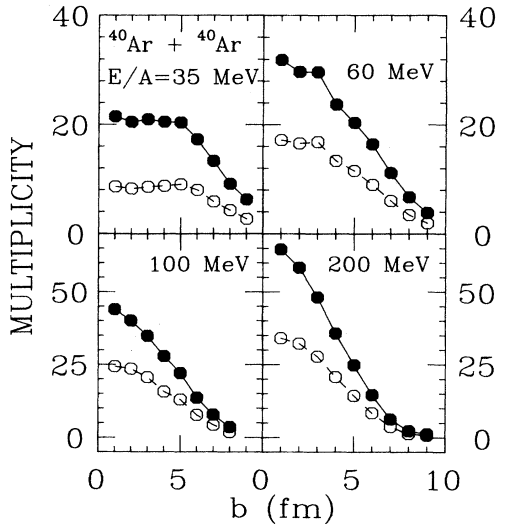

FIG. 28. Total nucleon multiplicities are given by the solid points and the multiplicities of nucleons at $\theta<30°$ by the open points for the $^{40}Ar+^{40}Ar$ reaction at bombarding energies $E/A=35$, 60, 100, and 200 MeV. The lines are drawn to guide the eye.

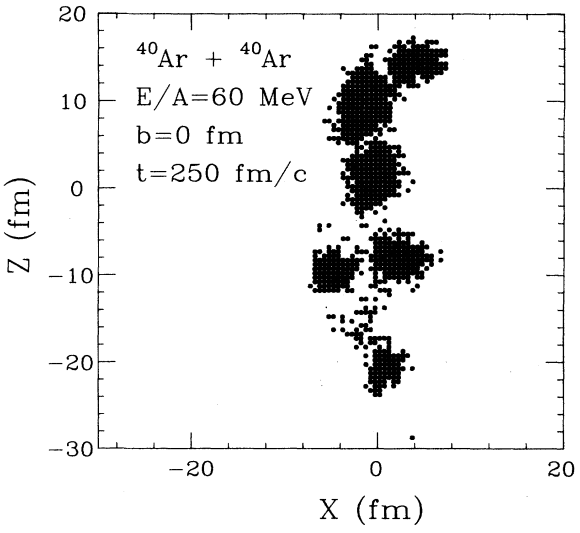

FIG. 27. The locations of bound test particles calculated with the Boltzmann equation are shown after an elapsed time of 250 fm/c for the $^{40}Ar+^{40}Ar$ reaction at $E/A=60$ MeV and zero impact parameter. The locations of unbound test particles are not plotted in these figures.

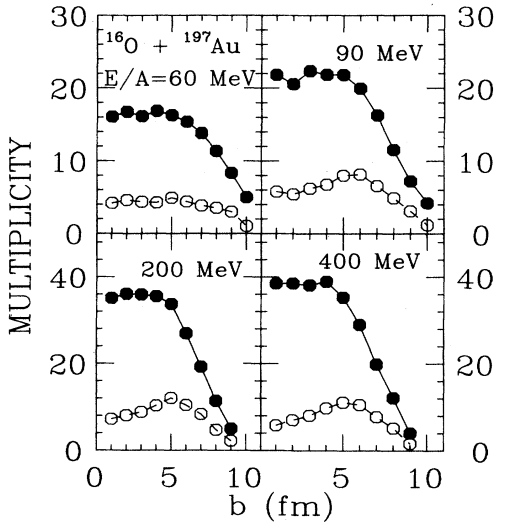

FIG. 29. Total nucleon multiplicities are given by the solid points and the multiplicity of nucleons at $\theta<30°$ by the open points for the $^{16}O+^{197}Au$ reaction at bombarding energies $E/A=60$, 90, 200, and 400 MeV. The lines are drawn to guide the eye.

teresting to note that the impact-parameter dependences of both the calculations at $E/A=200$ and 400 MeV are qualitatively similar to those displayed for the $^{16}O+^{197}Au$ reaction at $E/A=90$ MeV. Such dependences are different from those predicted for collisions between mass-asymmetric systems at lower energies. These calculations suggest that multiplicity measurements may provide more quantitative impact-parameter information at small impact parameters for collisions at and above $E/A \approx 90$ MeV than below.

IV. SUMMARY

Guided by solutions of the Boltzmann equation, we have explored the sensitivity of different experimental observables to the impact parameter. These calculations were motivated by the knowledge that many of the most interesting observables, like the transverse momentum or flow, are strongly impact-parameter dependent and therefore ambiguities in the impact parameters can prevent us from fully utilizing the experimental measurements. Although the present calculations indicate that nearly all observables are sensitive to the impact parameter, a single reaction variable does not suffice to provide impact-parameter selection in general. Instead, we can identify reaction variables which provide impact-parameter selection for the different domains of incident energy and impact parameters.

For mass-asymmetric entrance channels like the $^{16}O+^{197}Au$ reaction, the average total nucleon multiplicity and the velocity of the reaction residue display a very similar dependence on the impact parameter. At low energies $E/A \leq 60$ MeV where the multiplicity is low and the existence of a reaction residue is assured, the residue velocity provides more accurate impact-parameter information because it is not subject to the statistical fluctuations of multiplicity measurements when the mean multiplicities are small. Unfortunately, for low-energy collisions, both residue velocity and multiplicity are insensitive to impact parameters for $b \lesssim 5$ fm. (Additional calculations are needed to determine whether the inclusion of the yields of particles evaporated from the highly excited target residue, not taken into account by the present calculations, can significantly improve the impact-parameter sensitivity of the multiplicity distributions.) At these smaller impact parameters, only the angular momentum of the reaction residue is impact-parameter dependent, suggesting that conventional techniques like the measurement of the γ ray multiplicity should be explored to see if they could provide additional information about the impact parameters.

For the $^{40}Ar+^{40}Ar$ system at $E/A=35$ MeV, the calculations suggest that compound nuclei are not formed at impact parameters greater than or equal to 2 fm; the nucleon multiplicity is sensitive to the impact parameter only for large impact parameters, $b>5$ fm. It is likely that similar results would be obtained for calculations with other symmetric systems.

At higher energies, where the existence of a reaction residue is questionable and needs experimental verification, the calculations suggest that the total nucleon multiplicity and the angular distribution of emitted nucleons may be combined to provide impact-parameter selectivity. This selectivity exists for symmetric systems at $E/A \geq 60$ MeV and for asymmetric systems at $E/A \geq 90$ MeV, and extends to rather small impact parameters. The distinction between different impact parameters will be somewhat blurred, however, by the effects of multiplicity fluctuations.

The values of some of the important parameters of the Boltzmann equation, like the velocity and density dependence of the nucleon-nucleon cross section and the nuclear mean field are not very well established. For intermediate energy collisions, uncertainties in the nucleon-nucleon cross section are probably more important. For the $^{14}N+^{154}Sm$ reaction we have shown that these uncertainties can strongly affect the calculated observables. In particular, the mean transverse momentum and the enhancement of emission patterns in the reaction plane are rather sensitive to the importance of nucleon-nucleon collisions. Uncertainties in the cluster production mechanism presently make the comparison of these observables to experimental data somewhat tenuous. These assumptions, however, clearly can and will be refined as more experimental data become available.

This work was supported by the National Science Foundation under Grant Nos. PHY-86-11210 and PHY-87-14432, and a U.S. Presidential Young Investigators Award.

[1]A. I. Warwick, H. H. Wieman, H. H. Gutbrod, M. R. Maier, J. Peter, H. G. Ritter, H. Stelzer, and F. Weik, Phys. Rev. C **27**, 1083 (1983).

[2]H. A. Gustafsson, H. H. Gutbrod, B. Kolb, H. Löhner, B. Ludewigt, A. M. Poskanzer, T. Renner, H. Riedesel, H. G. Ritter, A. Warwick, F. Weik, and H. H. Wieman, Phys. Rev. Lett. **52**, 1590 (1984).

[3]M. Jääskeläinen, D. G. Sarantites, R. Woodward, F. A. Dilmanian, J. T. Hood, R. Jääskeläinen, D. C. Hensley, M. L. Halbert, and J. H. Barker, Nucl. Instrum. Methods **204**, 385 (1983).

[4]D. G. Sarantites, J. H. Barker, M. L. Halbert, D. C. Hensley, R. A. Dayras, E. Eichler and N. R. Johnson, and S. A. Gronemeyer, Phys. Rev. C **14**, 2138 (1976).

[5]J. Galin, Nucl. Phys. **A488**, 297c (1988).

[6]U. Jahnke, G. Ingold, H. Homeyer, M. Burgel, Ch. Egelhaaf, H. Fuchs, and D. Hilscher, Phys. Rev. Lett. **50**, 1246 (1983).

[7]Z. Chen, C. K. Gelbke, J. Pochodzalla, C. B. Chitwood, D. J. Fields, W. G. Gong, W. G. Lynch, and M. B. Tsang, Nucl. Phys. **A473**, 564 (1987).

[8]T. C. Awes, G. Poggi, C. K. Gelbke, B. B. Back, B. G. Glagola, H. Breuer, and V. E. Viola, Jr., Phys. Rev. C **24**, 89 (1981).

[9]L. W. Nordheim, Proc. R. Soc. London Ser. A **119**, 689 (1928).

[10]G. F. Bertsch, H. Kruse, and S. Das Gupta, Phys. Rev. C **29**, 673 (1984).

[11]J. Aichelin and G. Bertsch, Phys. Rev. C **31**, 1730 (1985).

[12]G. F. Bertsch and S. Das Gupta, Phys. Rep. **160**, 189 (1988).

[13]These values of nuclear mean field and the nucleon-nucleon

cross section are consistent with Ref. 11.

[14]B. A. Brown (private communication). The calculation used a spherical basis since deformation effects cannot be taken into account with the Thomas-Fermi approximation. The interaction employed in the paper was the SGII Skyrme-type interaction. Calculations with this interaction for the spherical ^{144}Sm nucleus are in excellent agreement with experimentally measured charge distributions. B. A. Brown, C. R. Bronk, and P. E. Hodgson, J. Phys. G **10**, 1683 (1984).

[15]G. F. Bertsch, W. G. Lynch, and M. B. Tsang, Phys. Lett. B **189**, 384 (1987).

[16]M. B. Tsang, C. B. Chitwood, D. J. Fields, C. K. Gelbke, D. R. Klesch, W. G. Lynch, K. Kwiatkowski, and V. E. Viola, Jr., Phys. Rev. Lett. **52**, 1967 (1984).

[17]M. Fatyga, K. Kwiatkowski, V. E. Viola, W. G. Wilson, M. B. Tsang, J. Pochodzalla, W. G. Lynch, C. K. Gelbke, D. J. Fields, C. B. Chtwood, Z. Chen, and T. Nayak, Phys. Rev. Lett. **58**, 2527 (1987).

[18]K. Hagel, D. Fabris, P. Gonthier, H. Ho, Y. Lou, Z. Majka, G. Mouchaty, M. N. Namboodiri, J. B. Natowitz, G. Nebbia, R. P. Schmitt, G. Viesti, R. Wada, and B. Wilkins, Nucl. Phys. **A468**, 429 (1988).

[19]M. B. Tsang, W. G. Lynch, R. M. Ronningen, Z. Chen, C. K. Gelbke, T. Nayak, J. Pochozalla, F. Zhu, M. Tohyama, W. Trautmann, and W. Dunnweber, Phys. Rev. Lett. **60**, 1479 (1988).

[20]M. B. Tsang, R. M. Ronningen, G. Bertsch, Z. Chen, C. B. Chitwood, D. J. Fields, C. K. Gelbke, W. G. Lynch, T. Nayak, J. Pochodzalla, T. Shea, and W. Trautmann, Phys. Rev. Lett. **57**, 559 (1986).

[21]A. Kyanowski, F. Saint-Laurent, D. Ardouin, H. Delagrange, H. Doubre, C. Grégoire, W. Mittig, A. Péghaire, J. Péter, Y. P. Viyogi, B. Zwieglinski, J. Québert, G. Bizard, F. Lefèbvres, B. Tamain, J. Pochodzalla, C. K. Gelbke, W. Lynch, and M. Maier, Phys. Lett. B **181**, 43 (1986).

[22]Z. Chen, C. K. Gelbke, W. G. Gong, Y. D. Kim, W. G. Lynch, M. Maier, J. Pochodzalla, M. B. Tsang, F. Saint-Laurent, D. Ardouin, H. Delagrange, H. Doubre, J. Kasagi, A. Kyanowski, A. Peghaire, J. Péter, E. Rosato, G. Bizard, F. Lefebvres, B. Tamain, J. Québert, and Y. P. Viyogi, Phys. Rev. C **36**, 2297 (1987); F. Saint-Laurent *et al.* (unpublished).

[23]M. Fatyga, K. Kwiatkowski, V. E. Viola, C. B. Chitwood, D. J. Fields, C. K. Gelbke, W. G. Lynch, J. Pochodzalla, M. B. Tsang, and M. Blann, Phys. Rev. Lett. **55**, 1376 (1985).

[24]W. Bauer G. F. Bertsch, and S. Das Gupta, Phys. Rev. Lett. **58**, 863 (1987).

[25]J. Aichelin, Phys. Rev. C **33**, 537 (1986).

[26]P. Danielewicz and G. Odyniec, Phys. Lett. **157B**, 146 (1985).

[27]E. C. Pollaco, M. Conjeaud, S. Harrar, C. Volant, Y. Cassagnou, R. Dayas, R. Legrain, H. Oeschler, and F. Saint-Laurent, Phys. Lett. **146B**, 29 (1984).

[28]M. Conjeaud, S. Harrar, M. Mostefai, E. C. Pollaco, C. Volant, Y. Cassagnou, R. Dayras, R. Legrain, H. Oeschler, and F. Saint-Laurent, Phys. Lett. **159B**, 244 (1985).

[29]A. Schwarzschild and C. Zupancic, Phys. Rev. **129**, 854 (1963).

[30]J. Pochodzalla, C. K. Gelbke, W. G. Lynch, M. Maier, D. Ardouin, H. Delagrange, H. Doubre, D. Geregoire, A. Kyanowski, W. Mittig, A. Peghaire, J. Péter, F. Saint-Laurent, G. Zwieglinski, G. Bizard, F. Lefebvres, B. Tamain, J. Québert, Y. P. Viyogi, W. A. Friedman, and D. H. Boal, Phys. Rev. C **35**, 1695 (1987).

[31]G. Bizard, A. Drouet, F. Lefèbvres, J. P. Patry, B. Tamain, F. Guilbault, and C. Lebrun, Nucl. Instrum. Methods **A244**, 483 (1986).

[32]M. B. Tsang, Y. D. Kim, N. Carlin, Z. Chen, R. Fox, C. K. Gelbke, W. G. Gong, W. G. Lynch, T. Murakami, T. K. Nayak, R. M. Ronningen, H. M. Xu, F. Zhu, L. Sobotka, D. Stracener, D. G. Sarantites, Z. Majka, V. Abenante, and H. Griffin, Phys. Lett. B (in press).

[33]D. Ardouin, Z. Basrak, P. Schuck, A. Péghaire, H. Delagrange, H. Doubre, C. Grégoire, A. Kyanowski, W. Mittig, J. Péter, F. Saint-Laurent, B. Zwieglinski, V. P. Viyogi, C. K. Gelbke, W. G. Lynch, M. Maier, J. Pochodzalla, J. Québert, G. Bizard, F. Lefèbvres, and B. Tamain, Z. Phys. A **329**, 505 (1988).

[34]D. Ardouin (private communication).